The FDTD Algorithm for Scattering from A Three-Dimensional Model of An Object over Random Rough Surface

Ya-Qiu Jin and Lei Kuang
Key Laboratory of Wave Scattering and Remote Sensing Information (Ministry of Education)
Fudan University, Shanghai 200433, China
Email: yqjin@fudan.ac.cn

Abstract

A numerical FDTD approach for electromagnetic scattering from an object over a randomly rough surface in three-dimensional (3D) model is developed. Rough surface is truncated in numerical simulation by using the periodic surface extension, and one period of the rough surface with dependence of the correlation length is used for scattering computation. Generation of the incident wave upon the rough surface is presented. A numerical model and algorithm of a single object on or above a rough surface are developed. Polarized bistatic scattering from the object and rough surface is obtained based on numerical distribution of the near zone fields. Comparison with conventional two-dimensional model is also discussed.

I. INTRODUCTION

Electromagnetic scattering from the composite model of the volumetric object and rough surface has been of interest for extensive applications of oceanic surveillance, land mine detection and so on. Conventional analytic approaches of rough surface scattering based on some approximations were unable to manage complicated interactions between the object and rough surface.

Due to the advance of computational technology, numerical approach of electromagnetic (EM) scattering for comprehensive volume-surface model has been extensively investigated. For example, numerical MOM [4]• FBM [5]• • GFBM [6,7]• FBM/SAA [8]• FEM [9,10] and Iterative Method [11,12] etc. have been applied to simulation of EM scattering from two-dimensional (2D) model of an object and rough surface. However, it is difficult to extend these approaches to three-dimensional (3D) case, since the unknowns of a 3D surface in numerical algorithm become extremely large.

In this paper, the rough surface is seen as a periodically extensive surface (shown in Fig.1). Because one period surface is illuminated by incident plane wave in the FDTD computation, it greatly reduces the unknown number and the memory cost. Then, a single 3D object is present over the rough surface, and near zone field interaction of both the object and rough surface is numerically calculated. Finally, bistatic scattering from the model of a volumetric object and rough surface is obtained by using the near-to-far fields transformation.

II. A PERIODIC ROUGH SURFACE

A randomly rough surface is seen as a periodically extensive surface as shown in Fig.1. Diffraction from the truncated surface edges is eliminated by using the periodicity condition. Thus, the study of scattering from infinite rough surface is simplified as a case of one periodic cell as shown by one square surface of Fig.1.

Using the Monte Carlo Method, a Gaussian randomly rough surface with given correlation length is generated.

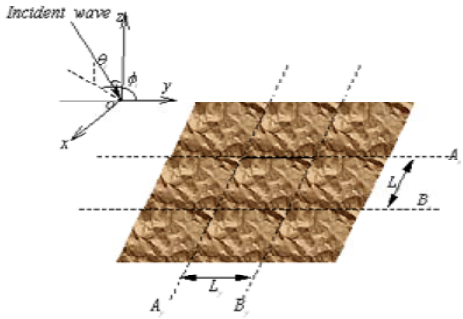

Fig. 1 A periodic rough surface.

A 3D Gaussian randomly rough surface is generated from the given spectral density and correlation function. To validate generation of the 3D rough surface, the correlation function (CF) of numerically generated rough surface is compared with previously given CF. The relative error of the *rms* height and the *rms* error of the CF for different surface sizes show that as analogous to 2D case, the 3D rough surface with $L_x \geq 15l_x$ and $L_y \geq 15l_y$ well satisfies the surface statistics. It leads that one period should satisfy

$$S \geq 15l_x \times 15l_y \tag{1}$$

In Fig. 2, the domain $A''B''C''D''E''F''G''H''$ is the computation space and is truncated by anisotropic perfectly matched layer (PML) [15] for absorbing the outward-propagating waves.

Incident wave is generated on the upper and four sides of

the region $ABCDEFGH$. The computation region under consideration is now inside the periodic interfaces, where the regions of total field and scattered field are computed, respectively, below and above the surface $EFGH$.

To apply FDTD, the rough surface is divided into the Yee space lattices. The parameters of PML above and below the rough surface are chosen, separately, to make no reflections from the PML interfaces.

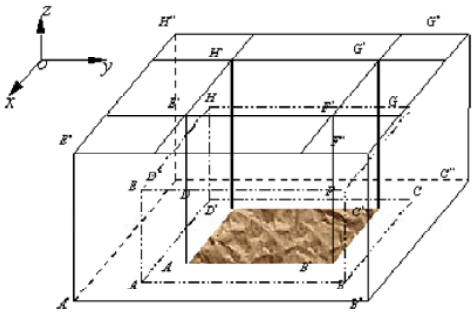

Fig. 2 A FDTD model of rough surface.

Using the periodic boundary condition (PBC), the fields of the points in an infinite space along the periodic directions on x-y plane can be readily described by the fields of one period cell. For example, as indicated in Fig.1, a relationship of $B_y = A_y + L_y$ can yield the fields:

$$\psi(x, B_y, z, t) = \psi(x, A_y, z, t - L_y / v_y) \qquad (2a)$$

$$\psi(x, A_y, z, t) = \psi(x, B_y, z, t + L_y / v_y) \qquad (2b)$$

where v_y is the phase velocity along y direction.

The position of a field point in computation space is denoted as $(i, j, k) = (i\Delta x, j\Delta y, k\Delta z)$. Here Δx , Δy , Δz are, respectively, the lattice space increments in the x, y and z coordinate directions. As shown in Fig.1, the left and right periodic boundaries are located at $j = A_y$ and $j = B_y$. The outboard fields of the left (right) periodic boundaries can be expressed correspondingly by the inboard fields. The FDTD method combining with the periodic boundary condition, which has been implemented for frequency selective surfaces (FSS) structures [16], is employed for our periodic rough surface model.

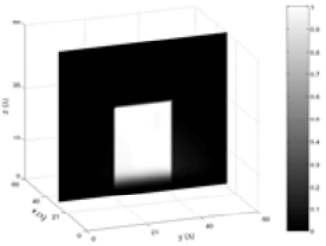

Fig. 3(a) Distribution of H_x .

To verify generation of the incident wave, an example of a TM plane wave with no object presence is shown in Figs. 3(a-c). It can be seen that only H_x, E_y, E_z exist in the total field region and their amplitudes are equal to corresponding incident field amplitudes. The fields decay to zero in PML region, and no field is released outside the total field region. It validates the incident wave generation.

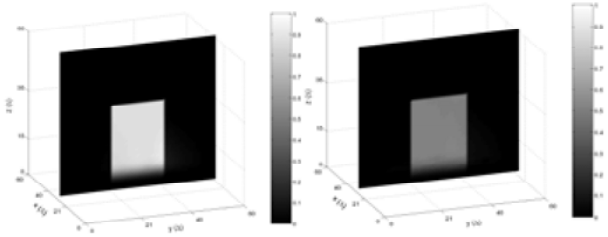

Fig.3(b) Distribution of E_y Fig.3(c) Distribution of E_z .

III. OBJECT-SURFACE INTERACTION

Now a single object is present on or over rough surface. Scattering mechanism includes: (1) scattering from rough surface excited by incident wave, (2) scattering from the object excited by incident wave, and (3) scattering due to interaction between the object and rough surface.

The periodic boundary condition to eliminate edge effects cannot be simply implemented. We first calculate the near zone field around the rough surface alone by using the periodic boundary condition (zone 1 in Fig.4). Then, this near zone field is employed as the excitation source for the model of the object and rough surface as shown by the model of Fig. 4(b) (zone 2 in Fig.4).

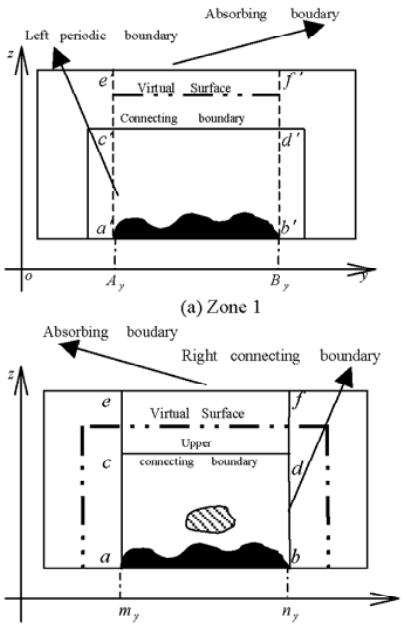

(a) Zone 1

(b) Zone 2

Fig.4 A FDTD model of an object and rough surface.

As an object is present, it is first illuminated by the excitation source. Then, scattering from the object is applied

to excite the underlying rough surface. And the object is also excited by the scattering from rough surface in turn. Thus multiple interaction scatterings between the object and rough surface are taken into account, and all scatterings from the object and rough surface are computed for each time step until the steady state is reached. The domain *abdc* is the total field region of the object and rough surface, where incident field is entirely confined. And scattered field from the rough surface excited by incident wave is confined within four sides connecting boundaries for all time.

Making use of the field of "zone 1" as the excitation source, the edge effects of the finite rough surface are eliminated and no periodicity of a single object would be introduced.

As a validation of computation code, an example of no object in "zone 2" is first used to show that the field distribution within the four sides connecting boundaries in "zone 2" is equal to one within the periodic boundaries in "zone 1".

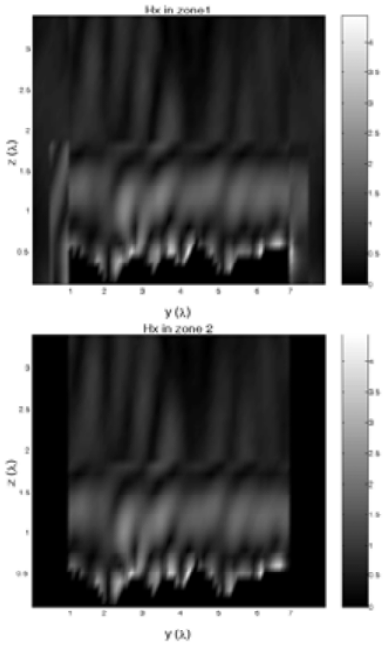

Fig.5 Comparison between H_x in "zone 1" and "zone 2".

Comparison shows good correspondence between the field distribution of rough surface in "zone 1" and that in "zone 2". It is found that no fields exist outside the four sides connecting boundaries in "zone 2".

IV. NUMERICAL RESULTS

Referring to [19], far zone scattered fields of rough surface can be computed in terms of the equivalent surface currents obtained by the tangential fields at the virtual surface over the rough surface (as zone 1 in Fig. 4). The same near-to-far field transformation is applied to obtain the far field of scattering from the object and rough surface. Here, the virtual surfaces (as zone 2 in Fig. 4) are settled in free space to semi-surround the object and underlying rough surface. Bistatic scattering coefficient [20] is defined as

$$\sigma_{qp} = \lim_{\rho\to\infty}\left(\frac{4\pi\rho^2\left|\vec{E}_q^s\right|^2}{\left|\vec{E}_p^i\right|^2 \cdot S\cdot\cos\theta_i}\right) \tag{3}$$

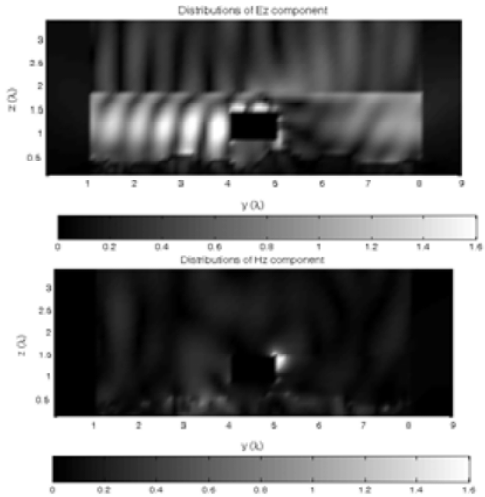

Fig. 6 Near fields of a rectangular box over rough surface.

It can be seen from Fig. 6(a) that the total fields are confined within the domain ($1\lambda \le y \le 8\lambda$, $z \le 1.8\lambda$), and the boundaries between the total field and scattered field from the object and rough surface are distinct. Note that the connecting boundaries in Figs. 6(a) and 6(b) can be identified, because scattering from the rough surface excited only by incident wave is confined within four side connecting boundaries and little scattered field exists outside the four sides. No boundary between the total field and the scattered field can be found in Fig. 6(b) due to no H_z for incident field of this example.

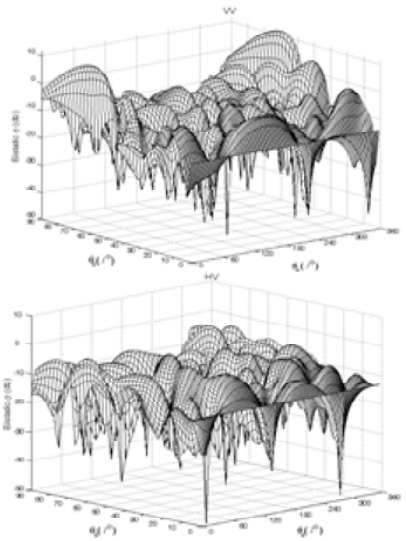

Fig. 7 Bistatic scattering from the object and rough surface.

Far fields are transformed from the near fields. Co-polarized (VV) and cross-polarized (HV) bistatic scattering coefficients are shown in Figs. 7(a,b), respectively.

Making the average of 10 realizations, bistatic VV and HV-polarized scattering coefficients are shown in Figs. 8(a,b).

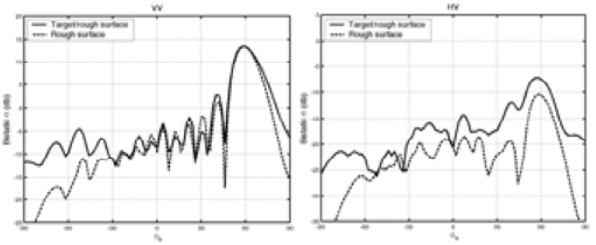

Fig.8 Bistatic scattering coefficient vs. scattering angle,

Comparing Figs. 8(a) and 8(b), it can be seen that co-polarized scattering is always stronger than cross-polarized in most scattering angles, and the scattering peaks occur in specular direction for both polarizations. When an object is present over rough surface, angular HV-polarized scattering is almost uniformly increased, and VV-polarized backscattering ($\theta_s = -60^o$) is especially enhanced. However, in this parameterized model the scattering from rough surface most likely governs angular pattern for both polarization.

Azimuthal variation of bistatic VV- and HV-polarized scattering coefficients are shown in Figs. 9(a,b), respectively. Angular pattern and enhancement of bistatic scattering due to the object presence is dependent upon the object size, shape, orientation and its height over rough surface.

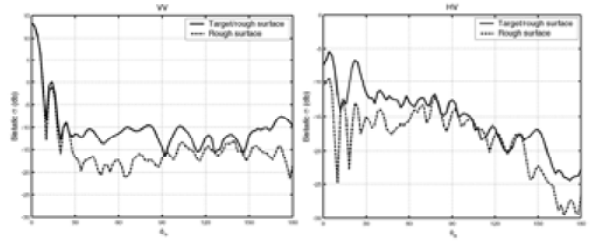

Fig. 9 Azimuthal variations of bistatic scattering coefficients

To infinitely extend the shape of the object and surface in the *x*-dimension, the 3D model is simplified to 2D case. To compare the 3D and 2D cases, suppose that a 3D object with the size $1\lambda \times 1\lambda \times 0.6\lambda$ over a rough surface with the area $7\lambda \times 7\lambda$ is equivalently transformed to a 2D object with the size $1\lambda \times 0.6\lambda$ and surface length $L = 49\lambda$ in such way:

$$\frac{\text{Cross section of 3D object}}{\text{Cross section of 3D rough surface}} = \frac{1\lambda \times 1\lambda \times \cos\theta_i + 0.6\lambda \times 1\lambda \times \sin\theta_i}{7\lambda \times 7\lambda \times \cos\theta_i}$$

should be equal to

$$= \frac{\text{Cross section of 2D object}}{\text{Cross section of 2D rough surface}} = \frac{1\lambda \times \cos\theta_i + 0.6\lambda \times \sin\theta_i}{49\lambda \times \cos\theta_i} = \frac{\cos\theta_i + 0.6\sin\theta_i}{49\cos\theta_i}$$

Comparison of bistatic VV scattering coefficients $\sigma_{vv}(\theta_s, \theta_i = 60^\circ, \phi_s - \phi_i = 0)$ (average of 10 realizations) for 3D and 2D cases is shown in Fig. 10. Angular scattering of these two cases keeps similarity, but the 2D model shows quicker and deeper oscillation. Because the rectangular object in this example is small comparing with the surface size, total scattering in the specular direction is actually dominated by the surface scattering. Since the object and surface dimensions of the 2D model are infinite along *x*-axis, it significantly enhances the specular reflection and backscattering, and shows quick oscillation.

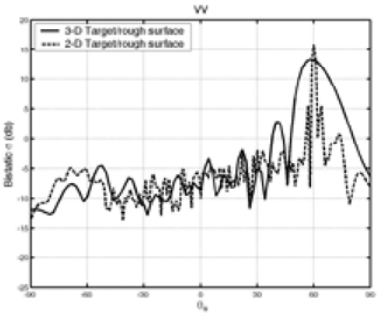

Fig.10 Bistatic scattering of 3D and 2D models.

ACKNOWLEDGMENT

This work was supported by the China Major Basic Research Project 2001CB309400 and NSFC 60571050.

REFERENCES

[1] N. Geng, M.A. Ressler, and L. Carin, "Wide-band VHF scattering from a trihedral reflector situated above a lossy dispersive halfspace," IEEE Trans. Geosci. Remote Sensing, 1999, 27(9): 2609-2617.

[2] J.T. Johnson, "A study of the four-path model for scattering from an object above a halfspace," Microwave Opt. Technol. Lett., 2001, 30(7): 130-134.

[3] Z.J. Liu, J.Q. He, Y.J. Xie, A. Sullivan and L. Carin, "Multilevel fast multipole algorithm for general targets on a half-space interface," IEEE Trans. Antennas Propag. , 2002, 50(12): 1838–1849.

[4] X.D. Wang, Y.B. Gan. and L.W. Li, "Electromagnetic scattering by partially buried PEC cylinder at the dielectric rough surface interface: TM case," IEEE Trans. Antennas and Wireless Propag. Lett., 2003, 2(2): 319–322.

[5] D. Holliday, et al., "Forward backward: A new method for computing low grazing angle scattering," IEEE

Transactions on Antennas Propagation, 1996, 44(2): 722-729.

[6] M. R. Pino, L. Landesa, J.L. Rodriguez, F. Obelleiro, and R.J. Burkholder, "The generalized forward-backward method for analyzing the scattering from targets on ocean-like rough surfaces," IEEE Trans. Antennas Propagat., 1999, 47(6): 961–969.

[7] Y.Q. Jin and Z. Li, "Numerical simulation of radar surveillance for the ship target and oceanic clutters in two-dimensional model", Radio Science, 2003, 38(3): 1045-1050.

[8] Z. Li and Y.Q. Jin, "Bistatic scattering and transmitting through a Fractal rough surface with high permittivity using the PBTG-FBM/SAA method", IEEE Transactions on Antennas and Propagation, 2002, 50(9): 1323-1326.

[9] P. Liu and Y.Q. Jin, "Numerical simulation of the Doppler spectrum of a flying target above dynamic oceanic surface by using the FEM-DDM method," IEEE Trans. Antennas Propag. , 2005, 53(2): 825–832.

[10] P. Liu and Y.Q. Jin, "Numerical simulation of bistatic scattering from a target at low altitude above rough sea surface under an EM wave incidence at low grazing angle by using the finite element method," IEEE Trans. Antennas Propag., 2004, 52(5): 1205–1210.

[11] H. Ye and Y.Q. Jin, "Fast iterative approach to difference scattering from the target above a rough surface," IEEE Trans. Geosci. Remote Sensing, 2006, 44(1): 108-115.

[12] H. Ye and Y.Q. Jin. "Parameterization of the tapered incident wave for numerical simulation of electro-magnetic scattering from rough surface," IEEE Trans. Antennas Propagation, 2005, 53(3): 1234-1237.

[13] J.T. Johnson, "A numerical study of scattering from an object above a rough surface," IEEE Trans. Antennas Propag., 2002, 50(10):1361-1367.

[14] J. J. Wu. "Simulation of rough surfaces with FFT," Tribology International, 2000, 33(1): 47-58.

[15] S. D. Gedney. "An anisotropic perfectly matched layer absorbing media for the truncation of FDTD lattices," IEEE Trans. Antennas Propagat., 1996, 44(12): 1630-1639.

[16] P. Harms, R. Mittra and W. Ko. "Implement of the periodic boundary condition in the finite-difference time-domain algorithm for FSS structures," IEEE Trans. Antennas Propagat., 1994, 42(9): 1317-1324.

[17] Anantha V. and Taflove A. "Efficient Modeling of infinite scatters using a generalized Total-Field/ Scattered-Field FDTD boundary partially embedded within PML," IEEE Trans. Antennas Propagat., 2002, 50(10): 1337-1349.

[18] Taflove A. "Computational Electromagnetics: The Finite Difference Time Domain Method," Norwood, MA: Artech House, 1995, 197-224.

[19] A.K. Fung, M.R. Shah and S. Tjuatja. "Numerical simulation of scattering from three-dimensional randomly rough surfaces," IEEE Trans. Geoscience and Remote Sensing, 1994, 32(5): 986-994.

[21] L. Tsang and J.A. Kong. Scattering of Electromagnetic Waves (vol. 1: Theories and Applications). John Wiley & Sons Inc., New York, 2001, 66-68.